SCIENTIFIC JOURNAL
EARTH'S CRYOSPHERE

Earth's Cryosphere, 2016, vol. XX, No. 4, pp. 26–33 **http://earthcryosphere.ru/**

GEOCRYOLOGICAL MONITORING AND PREDICTION

PREDICTED CHANGES IN STOCKS OF SOIL ORGANIC CARBON UNDER THE MODERATE CLIMATE SCENARIO FOR NORTHERN EUROPEAN RUSSIA

A.V. Pastukhov

Institute of Biology, Komi Science Center UB RAS,
28, Kommunisticheskaya str., Syktyvkar, 167982, Russia; alpast@mail.ru

Predictive assessment of the regional soil organic carbon stocks has been carried out for the tundra and forest tundra in the northeastern part of European Russia. The obtained regional matrices and maps account for 83 % of the changes in soil organic stocks depending on the environmental factors (combined soil taxa, terrain dissection, and climate characteristics – temperature and precipitation), with the calculations based on the moderate climate scenario E-GISS. According to the prediction model (excluding the environmental inertia) the resulting soil organic carbon stocks will decrease by 1.27 kg/m^2 (–3.47 %) in 2050, i.e. soil organic carbon is predicted to be 35.29 kg/m^2, whereas current soil organic carbon stocks are estimated 36.56 kg/m^2.

Predictive modeling, stocks, soil organic carbon, moderate climate scenario

INTRODUCTION

Soil organic carbon (SOC) pool is the largest constituent in terrestrial biosphere [*Jobbagy and Jackson, 2000*], therefore its mineralization due to climate warming will speed the rise of CO_2 concentrations in the atmosphere. Soil carbon losses are determined by variations in temperature [*Davidson and Janssens, 2006*], moisture [*Ryan and Law, 2005*], and the levels of soil disturbance resulting from land management [*Post and Kwon, 2000*], and wildfires [*Harden et al., 2000*]. Because of their high vulnerability to climate changes, these factors largely contribute to feedback synergies capable of speeding or slowing down accumulation of greenhouse gases into the atmosphere [*Young and Steffen, 2009*]. The pool of SOC stored in permafrostregions is very large [*Tarnocai et al., 2009*] and potentially labile following ongoing climate change [*Zimov et al., 2006; Schuur et al., 2008*]. According to most recent climate change scenarios, there's expected a 4–7 °C increase in the mean temperature in the northern European Russia, and precipitation shows an upward trend in the amount in winter for the end of the 21st century [*Giorgi, 2006*].

Average estimates of SOC pool for the Arctic tundra and forest tundra calculated by different authors differ by several times. These ecoregions can potentially actively exert their influence on the ongoing climate changes due to huge SOC stocks and the rapid thawing of permafrost [*Schuur et al., 2008*], therefore monitoring of SOC spatial distribution is critical for correct estimates of its stocks. A great variety of integrated models for SOC stocks spatial distribution pattern and their dynamics have been actively developed and tested, recently [*Lawrence et al., 2008; Koven et al., 2011; Schaefer et al., 2011*].

Nevertheless, there are huge differences between estimates obtained through the modeling and experimentally, primarily due to a low spatial resolution and rough extrapolation of a limited number of observations. In addition, all models have a number of drawbacks: the lack of vertical resolution in SOC stocks[1], unrealistic spatial representation of the diversity of soil cover, in conjunction with largely neglected specificity of soil-forming processes conditions at high latitudes (cryogenic aggregation, podzolization, gleying, cryoturbation etc.). Despite these limitations, simulation techniques are often employed for predicting the changes in SOC stocks induced by climate fluctuations. Depending on the model processes and input parameters, permafrost carbon loss estimates resulted from different potential warming scenarios range widely (e.g., $25 \cdot 10^{12}$–$85 \cdot 10^{12}$ kg) [*Koven et al., 2011*].

The "reference" values for SOC stocks (mean values for soil taxonomic unit) are spatially non-uniform for larger (>100 km) regions, therefore, both climate and topography are needed to be taken into

[1] For example, carbon stocks in some models are calculated for soil layer with thickness 1 m, while in peatlands it can be several meters, which will remarkably impair SOC stock estimates.

account for adequate assessment of SOC stocks in these regions. Given that carbon sequestration is largely controlled by the environmental factors (soils, topography, climate), it is essential to use these by creating time series forecasting in addition to spatial models for prediction of SOC stocks. The previous studies [*Pastukhov, 2016*] revealed a close relationship between SOC stocks and environmental factors (combined soil taxa, mesorelief, climate characteristics) with determination coefficient $R^2 = 0.840$, and statistically significant results $p < 10^{-6}$. This high correlation resulted from environmental research suggests that SOC stocks are directly controlled by these factors [*Pastukhov et al., 2012*]. Unlike "pure" simulation models, for spatial modeling, we use real field data rather than theoretical approaches. Firstly, this minimizes bias in modeling, and secondly, allows an empirical substantiation of model upscaling for a wider geographic generalizations.

This paper concerns not only with modeling the current SOC stocks, but we also have computed spatial-temporal generalized linear models (GLM) for SOC stocks, which served as a basis for the raster prediction maps built for changes of SOC stocks under moderate climate scenario E-GISS.

STUDY AREA

The "Usa" Site is located in the Usa River basin in the Northeast of European Russia and, which is characterized by a temperate continental, moderately cold climate. This area is predominated by accumulative glacial relief which, morphologically, is a rolling plain with absolute elevations (a.s.l.) of 60–190 m, overlain by thick Quaternary deposits. The hills (musyurs) are irregularly shaped, have long gentle slopes and flat-topped, often swampy summits. The lowlands surrounding the hills are also swampy. The river valleys represent floodplains and first above flood-plain terraces.

The study region is located within the bounds of the "tundra–forest tundra" ecotone underlain by continuous permafrost in the north and sporadic permafrost in the southern part. The formation of cryogenic microrelief is primarilly associated with the occurrence of permafrost. The hummocky and spotty-hummocky microrelief is developed almost ubiquitously in the flatlands and wetland depressions, however, it is exceedingly rare in the areas adjacent to drainage lines, on essentially steep slopes, on tundra meadows, and at lower levels of floodplains. Such extensive distribution of the microrelief determines high complexity of soil cover at the micro-level characterized by soil combinations (complexes), with soils succeeding each other at distances from tens of centimeters to a few meters. Furthermore, the formation of the microrelief in soils is controlled by cryoturbation processes, which bring about disturbances into the profile structure, and subsurface horizons enrichment in organic matter transported mechanically from topmost layers. The microrelief of peat plateaus develops on the transition type bogs. Permafrost-affected (due to permafrost occurring in first meter of the soil horizon) and non-permafrost (permafrost occurs deeper than 1 m from the soil surface) soils have a fundamentally different thermal regime, even if they are separated by a distance of only several tens of meters [*Mazhitova and Kaverin, 2007*].

The mean annual soil temperature (MAST) range from −0.5 to −2 °C. The northern part of the study area ("Rogovaya 1" Site) is characterized by continuous permafrost, with thickness measuring considerably (up to 63–68 m), while the mean annual ground temperature (MAGT) is indicative of "warm permafrost", either approaching 0 °C, or falling down to −2.5 °C when it underlies peatlands and leeward slopes.

Thawed windows (taliks) are confined to river- and stream-channels, and probably to large lake basins. The configuration of the permafrost table is complex due to a variety of involved factors: vegetation, lithology, distance from water bodies and watercourses, hydrogeological regime, snow cover thickness, type of landforms, etc. The areas of anchored and non-anchored type of permafrost alternate, with the latter dominating. The ecotone sites comprise major patterns of treeline and cryolithozone extent and are therefore exceedingly vulnerable to climate change. They also include extensive relict peat plateau from Holocene climatic optimum and thermokarst complexes [*Pastukhov and Kaverin, 2013*].

These areas facilitate transition from shrub and dwarf birch tundra to thin forest-tundra grading into to the sparse northern taiga forests, whereas the structure and composition of plant communities are determined by the environment (solar and wind exposure, thickness of snow cover, the depth of permafrost occurrence). The treeline in permafrost-affected areas is usually delineated along non-permafrost river valleys, with sparse spruce growing directly on Cryosols at shallow (<1 m) occurrence of permafrost in the Bolshaya Rogovaya river basin.

The northern limit of tree-line is dominated by *Picea obovata* along with *Betula pubescens*. Shrubby *Salix* sp. and grasses are most evident along streams and swampy lowlands. Open fens and relict peat plateaus with thermokarst complexes are typical for the area. Non-permafrost fens are predominantly overgrown with *Sphagnum* sp., while peat plateaus (palsas and relict peat mounds) tend to be dominated by subshrubs, mosses and lichens. Deciduous shrubs or *Betula nana*, lichens and mosses thrive in open spaces of the tundra.

Seasonally-frozen (non-permafrost) soils (Gleysols, Cambisols, Retisols) develop typically under high bushes or forest vegetation where snow cover is

thick in winter, which ensures a warmer temperature regime of soils. Seasonally-frozen Fluvisols also develop on the floodplains of the river valleys [*Mazhitova et al., 2003*].

Peat plateaus of thermokarst complexes are characterized by Cryic Folic Histosols complexes with shallow occurrence of permafrost, and by seasonally frozen Fibric Histosols in fens, and Fibric Floatic Histosols, developing in thermokarst lake basins colonized by vegetation. Permafrost mineral soils (Cryosols), as a rule, form on the windward silty clay tundra landscape overgrown by subshrub vegetation, where thin snow cover benefit deeper cooling of soil and permafrost persistency in the profile [*Mazhitova et al., 2003*]. In the transition zones and small-scale elements of landscape, thick (10–40 cm) peat (organogenic) horizons (Histic Cryosols, Histic Gleysols) also contribute to permafrost preservation. Permafrost soils – Cryosols, Cryic Histosols – predominate in the zone of continuous permafrost of the northeastern part of the "Usa" Site.

This study is underpinned by the purposefully compiled database containing descriptions of all available profiles for the middle reaches of the Usa River basin, and reliable data on SOC stocks, as well as descriptions of vegetation and soils in WRB (World Reference Base) [*IUSS, 2014*].

The major sources are: 1) database of Institute of Biology, Komi Science Center UB RAS, used for the first time by P. Kuhry and co-authors [*Kuhry et al., 2002*] and by G. Mazhitova and co-authors [*Mazhitova et al., 2003*]; 2) database, compiled under the 2007–2008 CarboNorth project, and utilized by Hugelius and co-authors [*Hugelius et al., 2011*], and by *A. Pastukhov and D. Kaverin* [*2013*].

Sampling sites included four small key areas in the transition zone of the "tundra–northern taiga" ecotone in the middle reaches of the Usa Rv. basin. Sampling points were selected randomly, however, hummocks or depressions were carefully avoided. For more comprehensive understanding of the upper organic horizons thickness variability, controlled by the micro-relief parameters, the sampling was done in triplicate (except peatlands). The selection methodology, laboratory analyses, and calculations of SOC stocks are described in great detail in [*Hugelius et al., 2011*] or [*Pastukhov and Kaverin, 2013*]. The 1:300 000 digital soil map with resolution of 15 soil subgroups (according to WRB classification) was generated for the middle Usa river comprising the study area of 18 132.55 km^2 [*IUSS, 2014*]. This soil map was used for assessment of the current and predicted SOC stocks in the Usa Rv. basin. All soil groups and subgroups (WRB classification) were divided into three taxonomic classes differentiated by the organic horizons thicknesses.

Organogenic horizons is the main source for SOC stocks replenishment. Their average carbon content ranges generally between 30 and 35 %, whereas in mineral horizons it is less than 1 %. Therefore, the first combined taxonomic class included Histosols soil group (thickness of organogenic horizons: >40 cm), with SOC stocks estimates are remarkably high therein. Other soil groups feature a great variability in carbon stocks, however, they can be grouped into two soil taxa by the organogenic horizon thicknesses.

The first taxon includes mineral soils with organogenic horizons varying from 0 to 10 cm, while the latter includes 10 to 40 cm thick layers of peaty-mineral soil. Both modeling and predictive mapping for SOC stocks changes in space and time benefit greatly from Multiple Regression generalized linear model (GLM) [*Montgomery and Peck, 1982; McCullagh and Nelder, 1989*]. In the models, SOC stocks are viewed as a response dependent on such independent variables as combined taxa soils, climate and terrain characteristics. The information on climate data layers comes from the WorldClim [*Hijmans et al., 2005*; http://www.worldclim.org]. They have high resolution (30″), obtained by interpolation and extrapolation of data from 47,554 precipitation-monitoring and 24,542 temperature-monitoring weather stations (except Antarctica).

Spatial resolution of the GMTED2010 relief data of 15″ resolution in plan were provided by USGS [*Danielson and Gesch, 2011*]. Calculations of basic primary and secondary terrain attributes and statistical analyses were performed using the "Analytical GIS Eco" and R2 software packages developed by P.A. Shary [*Shary et al., 2002, 2011; Shary, 2008*].

A moderate climate scenario was used for projected changes in quantity of SOC stocks. E-GISS is the mean moderate model of NASA's Goddard Institute for Space Research. The global annual temperature averaged 14.6 °C in 2012, which is 0.6 °C warmer than mid-20th century. The global mean annual temperature has increased by 0.8 °C since 1880 (according to data from 1000 weather stations).

The collected data were used to build the GML equations of regression written as:

$$f(W) = aA + bB + cC + dD + e + \varepsilon,$$

where W is response (SOC stocks); A, B, C, D – predictors; a, b, c, d, e – regression coefficients; ε – error; $f(W)$ – link function, which corrects error distribution, and obeys the normal probability law.

CALCULATIONS OF PROJECTED VARIATIONS IN SOC STOCKS

The forecast for global climate fluctuations-driven SOC stocks changes in the tundra and forest-tundra soils in the northeast of European Russia, was carried out in several stages.

I. ***Construction of spatial model of SOC stocks, using integrated climatic characteristics – sums of precipitation and temperatures – as predictors***.

1. Spatial model of SOC stocks with total rainfalls in July and June operating as a spatial predictor for, has the form of [*Pastukhov, 2016*]

$$\ln(\mathrm{SOC})_{A110} = 0.026\,26 \cdot I_1 P_{\mathrm{Jul}+16.92} - 0.1617 \cdot P_{\mathrm{Jun}-5.29} -$$

$$- 0.003\,690 \cdot I_2 Z_{-4.17} + 0.042\,25 \cdot I_2\, rot^{\mathrm{P}}_{+2.66} + 8.487, (1)$$

$$R^2 = 0.840\ (Degr = 1.5\ \%),\ p < 10^{-6},$$

where ln – natural logarithm; A_{110} – sample set from 110 averaged observation points with estimated SOC stocks; 0.026 26, –0.1617, –0.003 690, 0.042 25 – regression coefficients; I_1, I_2 – predictors, designating organogenic and mineral soils including 0–10 cm thick organogenic horizon, respectively; lower indices +16.92, –5.29, –4.17, +2.66 are the values of *t*-statistics[2]; P_{Jul}, P_{Jun} – sum of the July–June rainfall; *Z* – altitude above sea level (a.s.l.); rot^{P} – one of the modifications of superscript "P" morphometric values[3], representing relief desiccation.

The model is log-normalized, as it takes into account a substantial deviation of statistical SOC distribution from normal distribution, which is associated with the specific role played by soil taxa in the context of this region. The model was verified by Allen cross-validation method using degradation criterion (*Degr*), which equals to 1.5 %, with the assumption that in ecology studies and soilscience 50 % is an acceptable level [*Shary et al., 2011*].

Model (1) shows that as many as 84 % of spatial distribution of SOC stocks ln (SOC) is controlled by soil taxa, climate characteristics (the sum of June P_{Jun} and July P_{Jul} rainfall) and relif (*Z* – a.s.l., *rot* – relief dissection); all predictors are significant in the model, i.e. difference between peatlands (Histosols) and other soil taxa was critical (by I_1 indicator organogenic soils is distinguished from any other soil taxa). Other critical factors were responsible for: the amount of rainfall in June P_{Jun}, term $I_2 Z$ accounting for elevation, and term $I_2 rot^{\mathrm{P}}$ accounting for relief dissection. This equation is used for calculations of SOC stocks spatialdistribution.

2. Spatial model of SOC stocks, using total amount of rainfall in June (P_{Jun}) and maximum July temperature $T^{\max}_{\mathrm{Jul}}$ as spatial predictors takes the form

$$\ln(\mathrm{SOC})_{A110} = 0.074\,873\,4 \cdot I_1 T^{\max}_{\mathrm{Jul}+16.29} -$$

$$-0.170\,931 \cdot P_{\mathrm{Jun}-6.08} - 0.018\,450\,4 \times$$

$$\times I_2 T^{\max}_{\mathrm{Jul}-3.95} + 0.041\,644\,1 \cdot I_2\, rot^{\mathrm{P}}_{+2.57} + 8.880\,005, (2)$$

$$R^2 = 0.833\ (Degr = 1.5\ \%),\ p < 10^{-6}.$$

It follows from model (2) that 83.3 % of spatial variability ln (SOC) is accounted for by soil taxa, climate (maximum July temperature $T^{\max}_{\mathrm{Jul}}$ and total rainfall in June P_{Jun}) and the relief dissection. First predicator $I_1 T^{\max}_{\mathrm{Jul}}$ proves the most significant and is related to peatlands alone: SOC stocks in peatlands tend to grow with increasing maximum July temperature. For linear pair correlation between $I_1 T^{\max}_{\mathrm{Jul}}$ and ln (SOC) has $R^2 = 0.741$. The sum of June precipitation P_{Jun} and term $I_2 rot^{\mathrm{P}}$ (accounting for local relief dissection) continue to operate as key factors. Term $I_2 T^{\max}_{\mathrm{Jul}}$, accounting for maximum July temperature for mineral soils, replaces $I_2 Z$. Determination coefficient in equation (2) is much lower than for model (1), however, given that apart from precipitation characteristics it is essential to take into account temperature variations, we will be using model (2) for calculations of projected changes in SOC stocks.

3. Spatial model of SOC stocks using total amounts of rainfall in July and June, included in equation (1), and the maximum July temperature as spatial predictors takes the form

$$\ln(\mathrm{SOC})_{A110} = -0.003\,648\,12 \cdot I_1 (P_{\mathrm{Jul}} - 23.37 \times$$

$$\times T^{\max}_{\mathrm{Jul}-16.24}) - 0.165\,592 \cdot P_{\mathrm{Jun}-5.87} - 0.018\,520\,7 \times$$

$$\times I_2\ T^{\max}_{\mathrm{Jul}-3.95} + 0.041\,421\,1 \cdot I_2\, rot^{\mathrm{P}}_{+2.55} + 8.664\,110, (3)$$

$$R^2 = 0.833\ (Degr = 1.5\ \%),\ p < 10^{-6}.$$

Model (3) replicates all predictors of model (2) except for the first one, where instead of $I_1 T^{\max}_{\mathrm{Jul}}$ we used $I_1(P_{\mathrm{Jul}} - 23.37 \cdot T^{\max}_{\mathrm{Jul}})$ – the invariant, or steady combination of the July rainfall and maximum July temperature, calculated in a special program, in order to have the sum of rainfall of two months remaining in the prediction calculations and to add a temperature characteristic.

Equation (3) explains 83.3 % of spatial variability in ln(SOC) by soil taxa, the invariant of $T^{\max}_{\mathrm{Jul}}$ with the sum of amount of rainfall in July and relief dissection.

The determination coefficient in model (3) being slightly lower than in (1), the most appropriate use of this model (3) would be for predictions, because apart from the July and June sum of precipitation it takes into account maximum July temperature as well both for peatlands and automorphic soils. For pair correlation of linear relationship between $I_1(P_{\mathrm{Jul}} - 23.37 \times \times T^{\max}_{\mathrm{Jul}})$ and ln (SOC) we obtain $R^2 = 0.744$.

II. ***Calculation of matrices for projected climate indicators.***

The calculation of the projected climate indicators matrices is based on the planetary data on tem-

[2] *t*-statistics depend on selected level of significance (elsewhere below $p = 0.05$) and number of degrees of freedom $n - k - 1$, which is 105 elsewhere below ($n = 110$ – sampling size; $k = 4$ – number of predictors).

[3] Given that statistical analysis involves spatial normalization of morphometric data, their values were modified according to formulas by P. Shary [*Shary et al., 2002*].

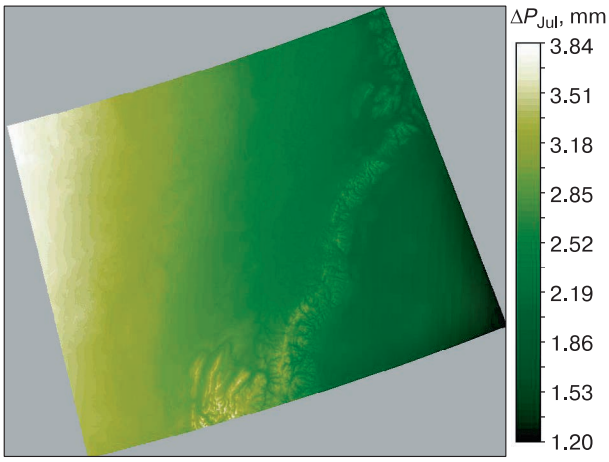

Fig. 1. Map (matrix) of variations in the sums of monthly rainfall for July 2050 (ΔP_{Jul}, mm) based on results of prediction model (4) and climate change scenario E-GISS.

perature and precipitation variations from the NASA website (Goddard Center) with grid step 4 × 5° in TXT format. With the use of the "Analytical GIS Eco" software the data are converted into its internal REG format.

Then, the data are interpolated with Delaunay method in several steps using the same software, to obtain matrix with lattice spacing 0.63°. The resulting matrix is converted into vector data (points), and finally into a given projection. A set of points with the predictive data is used as a response in the multiple regression equation, with the basic values of the related climatic indicators, geographic information, and terrain characteristics acting as variables.

The regression equation below describes the relationships of projected variations of sums of monthly rainfall for July 2050 according to E-GISS (ΔP_{Jul}_G50) scenario[4] with basic mean values of the sums of monthly rainfall for July (P_{Jul}_BASE), and coordinates X and $(X + Y)/2^{1/2}$:

$$\Delta P_{Jul}\_G50 = -1.505\,066 \cdot X - 0.539\,999 \cdot P_{Jul}\_BASE - \\ - 0.411\,735 \cdot (X + Y)/2^{1/2} + 3.743\,639, \qquad (4)$$

$$R^2 = 0.836, p < 10^{-6}.$$

In equation (4) the relationships are fairly strong (R^2 = 0.836). For the study region, the projected changes in sums of the July rainfall increase with decreasing basic main rainfall for July (P_{Jul}_BASE) moving west (longitude X with negative relationship) and southwest (variable $(X + Y)/2^{1/2}$ with a negative sign). The map of P_{Jul}_G50 changes built on the basis of the identified relationships is shown in Fig. 1.

The projected changes in the June rainfall pattern for 2050 according to E-GISS scenario (ΔP_{Jun}_G50) with basic mean values for rainfall in June (P_{Jun}_BASE), and X and $(X + Y)/2^{1/2}$ coordinates are described by the following model:

$$\Delta P_{Jun}\_G50 = -0.895\,675 \cdot X + 0.759\,441 \cdot (X + Y)/2^{1/2} + \\ + 0.645\,738 \cdot P_{Jun}\_BASE + 0.317\,421, \qquad (5)$$

$$R^2 = 0.415, p < 10^{-2}.$$

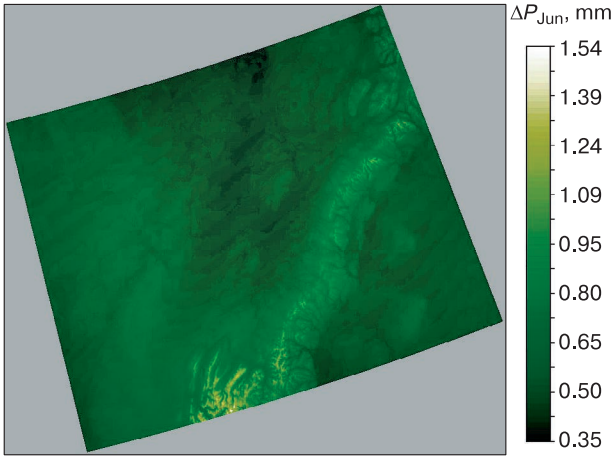

Fig. 2. Map (matrix) of variations in the sums of monthly rainfall for June 2050 (ΔP_{Jun}, mm) based on results of climate change prediction model E-GISS.

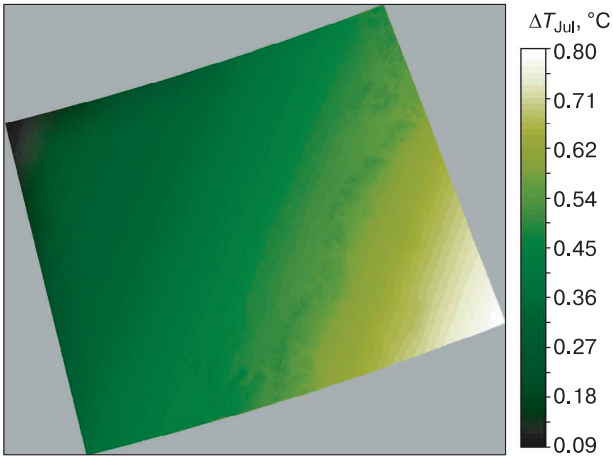

Fig. 3. Map (matrix) of variations in maximum July temperature for 2050 (ΔT_{Jul}, °C) based on results of climate change prediction model E-GISS.

[4] The ΔP_{Jul} G50 value – is difference between projected changes in the sum of the July rainfall for 2050 according to E-GISS scenario and basic mean (current) values of sum of the July rainfall.

In equation (5) for ΔP_{Jun}_G50 relationships appear weaker ($R^2 = 0.415$). The projected variations in sums of rainfall in June tend to grow with increasing basic mean sum of rainfall in June (P_{Jun}_BASE) moving west (longtitude X with negative sign) and to the northeast (variable $(X + Y)/2^{1/2}$ with negative sign). Map of P_{Jun}_G50 variations built according to equation (5) is shown in Fig. 2.

The model shown below describes relationships between projected changes in the E-GISS ($\Delta T^{\max}_{\text{Jul}}$_G50) scenario based maximum temperature of July for 2050 and basic mean maximum temperature values for July ($T^{\max}_{\text{Jul}}$_BASE), coordinates X and $(X - Y)/2^{1/2}$:

$$\Delta T^{\max}_{\text{Jul}}\text{G50} = 0.055\,02 \cdot T^{\max}_{\text{Jul}}\text{BASE} + 0.354\,284 \times$$

$$\times X + 0.207\,777 \cdot (X - Y)/2^{1/2} + 0.121\,935, \quad (6)$$

$$R^2 = 0.983,\ p < 10^{-6}.$$

In equation (6) relationships are very strong ($R^2 = 0.983$), which allows to infer that in the context of the study area, the projected variations in maximum temperature of July increase with growing basic mean temperature, moving east (variable X with positive sign) and south-east (variable $(X - Y)/2^{1/2}$ with positive sign). The resulting map of changes in $\Delta T^{\max}_{\text{Jul}}$_G50 based on the revealed relationships is shown in Fig. 3.

III. ***Calculation of changes in SOC stocks based on spatial models for the base period and forecasted temperature and precipitation data from the set of sampling points.***

The following average changes of climatic characteristics were calculated for 2050 using the E-GISS model through a set of samples (110 points) obtained using matrix maps (Fig. 1–3) for:

1) sum of rainfall in July (P_{Jul}) – an increase of (2.59 ± 0.04) mm from 54.38 mm (i.e. by 4.76 %);

2) sum of rainfall in June (P_{Jun}) – an increase of (0.43 ± 0.04) mm from 41.22 mm (i.e. by 1.05 %);

3) maximum July temperature ($T^{\max}_{\text{Jul}}$) – an increase of 0.41 °C from (18.89 ± 0.15) °C (i.e. by 2.15 %);

4) stable spatial compatibility between the sum of monthly rainfall in June and maximum July temperature ($P_{\text{Jul}} - 23.37 \cdot T^{\max}_{\text{Jul}}$) – compatibility decreases from –387.19 ± 3.55 to 6.89 (i.e. by 1.78 %).

By using equation (1), in which basic values P_{Jul} and P_{Jun} are substituted with predicted estimates in 110 points, we obtain:

1) average predicted SOC stocks in the study region are estimated 38.29 kg/m^2 for the year 2050;

2) average base SOC stocks estimate derived from equation (1) equals to 36.49 kg/m^2;

3) variations in the amount of SOC stocks are estimated to be +1.80 kg/m^2, or +4.92 % by the year 2050.

Calculations of changes in the amounts of SOC stock using the equation (1) without parametrization of environmental inertia (e.g. delayed turnover time in soil carbon processes) predict carbon sequestration in the soils of the study region by almost 5 %. The two "conflicting" predictors P_{Jul} and P_{Jun} (the former is with a positive sign in the model, while the latter is negative) in equation (1) indicate that an increase in the former is likely to cause an increase in SOC stocks, whereas an increase in the latter – a rise in emission rates.

Given that by 2050, according to the accepted scenario P_{Jul} will have grown by 4.76 %, while P_{Jun} – only by 1.05 %, the "conflict" is resolved in favor of a rise in emission. The average estimates of SOC stocks contained in soil taxa are given below: peatlands +5.72 kg/m^2 (or +6.58 %), mineral soils –0.02 kg/m^2 (or –0.18 %), peaty-mineral soils –0.02 kg/m^2 (or –0.09 %). Model (1) has predicted an increase in carbon stocks commensurable with an increase in sums of monthly rainfall in July for peatlands, while amount of SOC stocks will slightly decrease in other soil taxa.

Model (2), in which mean basic values for $T^{\max}_{\text{Jul}}$ and P_{Jun} are substituted with predicted estimates in 110 points, yielded the following results:

1) average projected SOC stocks are estimated to be 35.52 kg/m^2 by the year 2050;

2) average base SOC stocks based on equation (2) are estimated at 36.55 kg/m^2 for the year 2050;

3) variations in the amount of SOC stocks are expected to be –1.03 kg/m^2, or –2.82 % by the year 2050.

Model (2) not accounting for the environmental inertia either shows a potential almost 3 % decline or carbon emission in the soils of the study region. Equation (2) also has two "conflicting" predictors $I_1 T^{\max}_{\text{Jul}}$ (has positive relationship) and $I_2 T^{\max}_{\text{Jul}}$ (has negative relationship); in case the first predictor increases, the amount of SOC stocks is expected to grow, while an increase in the second predictor is predicted to cause a rise in emission. One more climatic predictor P_{Jun} is present in model (2), having negative influences on the SOC stocks. According to the accepted scenario, P_{Jun} will grow by 1.05 % by the year 2050, which results in the negative carbon budget. The average estimates of carbon fraction contained in soil taxa are as given below for: peatlands –1.53 kg/m^2 (or –1.91 %), mineral soils –0.68 kg/m^2 (or –5.89 %), peaty-mineral soils –0.91 kg/m^2 (or –5.20 %).

Model (2) forecasts an inconspicuous decrease in carbon stocks in peatlands, comparable to increased the sums of monthly rainfall in June (which tend to decrease SOC stocks in all the taxa) and a significant decrease in stocks in two other soil taxa.

Using model (3), where basic mean values of P_{Jul}, P_{Jun} and $T^{\max}_{\text{Jul}}$ are substituted with projected values in 110 points, we obtain the following results:

1) average predicted SOC stocks estimate in the study region is found to be 35.29 kg/m^2 by the year 2050;

2) average base SOC stocks estimate according to equation (3) equals to 36.56 kg/m^2;

3) variations in the amount of SOC stocks are estimated to be –1.27 kg/m^2, or –3.47 %.

Model (3) – without accounting for the environmental inertia – shows a potential decline by almost 3.5 % in SOC. In equation (3) we used the largest set of climate factors (P_{Jul}, P_{Jun} and T_{Jul}^{max}), acting as predictors. Given that their values are growing, this will cause a decrease in soil carbon throughout all the taxa. The average estimates of the carbon fraction contained in soil taxa are as given below for: peatlands –2.19 kg/m^2 (or –2.76 %), mineral soils –0.71 kg/m^2 (or –6.19 %), peaty-mineral soils –0.96 kg/m^2 (or –5.26 %).

CONCLUSIONS

Analysis of three spatial-temporal models with different climate predictors for one set of samplings and one predictive climate change scenario allowed to demonstrate how close the results are and assess the prediction robustness.

The calculation of changes in SOC stocks using equation (1) without taking into account the environmental inertia (regardless of the delayed turnover times) predicts an increase of carbon sequestration in soils of the study region by almost 5 %.

Model (2) not accounting for the environmental inertia either, predicts ca. 3 % reduction or emission of SOC in the soils of the studied region.

Model (3) taking no account of the environmental inertia predicts a decline in SOC stocks by almost 3.5 %.

The involvement of precipitation and temperature patterns into spatial-temporal models makes it possible to evaluate their synergies. In this research, all climatic predictors were statistically significant. Therefore model (3) appears interesting, accounting for two climate characteristics – totaled amounts of rainfall, and temperature. Model (1) has demonstrated the strongest relationship between the changes in SOC stocks and the environmental controls, which prove to be critical for spatial calculations. The results of model (3) projected a slight decrease in carbon stocks in soils (–3.47 %), comparable with variations in climate predictors, in percentage terms.

The author expresses his sincere appreciation to L.S. Sharaya and P.A. Shary for their assistance in practical application of his unique proprietary methodology and valuable comments on the paper, and to D.A. Kaverin for the joint field work and analytical studies and preparation of a soil map for the Usa river basin.

The research work was implemented within Project No. 15-2-4-28 "Biogeochemical processes as a base for Arctic soils sustainable functioning under changing environment (by the examples of low- and highland ecosystems)" within the 2015–2017 UB RAS Integrated Program.

References

Danielson, J.J., Gesch, D.B., 2011. Global multi-resolution terrain elevation data 2010 (GMTED2010). U.S. Geolog. Survey Open-File Rep. 2011-1073, 26 pp.

Davidson, E.A., Janssens, I.A., 2006. Temperature sensitivity of soil carbon decomposition and feedbacks to climate change. Nature, 440, 165–173, doi: 10.1038/nature04514.

Giorgi, F., 2006. Climate change hot-spots. Geophys. Res. Lett., vol. 33, iss. L08707, 1–4, doi: 10.1029/2006GL025734.

Harden, J.W., Trumbore, S.E., Stocks, B.J., et al., 2000. The role of fire in the boreal carbon budget. Glob. Change Biol. 6, 174–184, doi: 10.1046/j.1365-2486.2000.06019.x.

Hijmans, R.J., Cameron, S.E., Parra, J.L., et al., 2005. Very high resolution interpolated climate surfaces for global land areas. Intern. J. Climatol., vol. 25, 1965–1978, doi: 10.1002/joc.1276.

Hugelius, G., Virtanen, T., Kaverin, D., et al., 2011. High resolution mapping of ecosystem carbon storage and potential effects of permafrost thaw in periglacial terrain, European Russian Arctic. J. Geophys. Res., vol. 116, iss. G03024, 1–14, doi: 10.1029/2010JG001606.

IUSS Working Group WRB. 2014. World Reference Base for Soil Resources 2014. International soil classification system for naming soils and creating legends for soil maps. World Soil Res. Rep. No. 106, FAO, Rome, 2014, 191 pp.

Jobbagy, E.G., Jackson, R.B., 2000. The vertical distribution of soil organic carbon and its relation to climate and vegetation. Ecolog. Applications 10(2), 423–436, doi: 10.2307/2641104.

Koven, C.D., Ringeval, B., Friedlingstein, P., et al., 2011. Permafrost carbon-climate feedbacks accelerate global warming. Proc. Natl. Acad. Sci. USA, vol. 108, No. 36, 14769–14774, doi: 10.1073/pnas.1103910108.

Kuhry, P., Mazhitova, G.G., Forest, P.-A., et al., 2002. Upscaling soil organic carbon estimates for the Usa Basin (Northeast European Russia) using GIS-based landcover and soil classification schemes. Danish J. Geography, 102, 11–25.

Lawrence, D.M., Slater, A.G., Romanovsky, V.E., Nicolsky, D.J., 2008. Sensitivity of a model projection of near-surface permafrost degradation to soil column depth and representation of soil organic matter. J. Geophys. Res., vol. 113, iss. F02011, 1–14, doi: 10.1029/2007JF000883.

Mazhitova, G.G., Kaverin, D.A., 2007. Seasonal thaw depth and ground settlement at the Circumpolar Active Layer Monitoring Network (CALM) site in the European part of Russia. Kriosfera Zemli XI (4), 20–30.

Mazhitova, G.G., Kazakov, V.G., Lopatin, E.V., Virtanen, T., 2003. Geoinformation system for the Usa river basin (Republic of Komi) and calculations of soil carbon stocks. Pochvovedenie, No. 3, 133–144.

McCullagh, P., Nelder, J.A., 1989. Generalized Linear Models. Second ed. Chapman and Hall, London, 532 pp.

Montgomery, D.C., Peck, E.A., 1982. Introduction to Linear Regression Analysis. John Wiley & Sons, New York, 504 pp.

Pastukhov, A.V., 2016. Methodology for spatial modeling of soil organic carbon stocks in the north of European Russia. Earth's Cryosphere (Kriosfera Zemli) XX (3), 32–40.

Pastukhov, A.V., Kaverin, D.A., 2013. SOC stocks in the tundra and taiga ecosystems of the North-east Europe. Pochvovedenie, No. 9, 1084–1094, doi: 10.7868/S0032180X13070083.

Pastukhov, A.V., Sharaya, L.S., Sharyi, P.A., Kaverin, D.A., 2012. The spatial distribution of SOC in the forest tundra of the European North-East.Tenth Intern. Conf. on Permafrost: Northern Publ., Abstr. Salekhard, vol. 4, p. 443.

Post, W.M., Kwon, K.C., 2000. Soil carbon sequestration and land use change: processes and potential. Glob. Change Biol., vol. 6, 317–327, doi: 10.1046/j.1365-2486.2000.00308.x.

Ryan, M.G., Law, B.E., 2005. Interpreting, measuring, and modeling soil respiration. Biogeochemistry, vol. 73, 3–27, doi: 10.1007/s10533-004-5167-7.

Schaefer, K., Zhang, T., Bruhwiler, L., Barrett, A.P., 2011. Amount and timing of permafrost carbon release in response to climate warming. Tellus B., vol. 63, 165–180, doi: 10.1111/j.1600-0889.2011.00527.x.

Schuur, E.A.G., Bockheim, J., Canadell, J.G., et al., 2008. Vulnerability of permafrost carbon to climate change: implications for the Global carbon cycle. BioScience, vol. 58 (8), 701–714, doi: 10.1641/B580807.

Shary, P.A., 2008. Models of topography. Advances in Digital Terrain Analysis. Lecture Notes in Geoinformation and Cartography, XIV / Q. Zhou, B. Lees, G. Tang (Eds). Springer-Verlag, Berlin etc., pp. 29–57, doi: 10.1007/978-3-540-77800-4_3.

Shary, P.A., Rukhovich, O.V., Sharaya, L.S., 2011. Methodologic guidelines for analysis of spatial variability of wheat crop yield depending on the cultivated land conditions. Agrokhimia, No. 2, 57–81.

Shary, P.A., Sharaya, L.S., Mitusov, A.V., 2002. Fundamental quantitative methods of land surface analysis. Geoderma, 107 (1–2), 1–32, doi: 10.1016/S0016-7061(01)00136-7.

Tarnocai, C., Canadell, J.G., Schuur, E.A.G., et al., 2009. Soil organic carbon pools in the northern circumpolar permafrost region. Global Biogeochem. Cycles, vol. 23, iss. GB2023, 1–11, doi: 10.1029/2008GB003327.

Young, O.R., Steffen, W., 2009. The Earth System: Sustaining planetary life-support systems. Principles of Ecosystem Stewardship. Springer, New York, pp. 295–315.

Zimov, S.A., Davydov, S.P., Zimova, G.M., et al., 2006. Permafrost carbon: Stock and decomposability of a globally significant carbon pool. Geophys. Res. Lett., vol. 33, iss. L20502, 1–5, doi: 10.1029/2006GL027484.

Received April 30, 2015